JOURNAL OF NANO- AND ELECTRONIC PHYSICS
Vol. **18** No 2, 02023(6pp) (2026)

ЖУРНАЛ НАНО- ТА ЕЛЕКТРОННОЇ ФІЗИКИ
Том **18** № 2, 02023(6cc) (2026)

OPEN ACCESS

REGULAR ARTICLE

Material Dependent Variations in Nanoparticle Mediated Sensitization of Proton Irradiation

P. William[1,*], A. Verma[2,†], M. Almakki[3,‡], A.V. Brahmane[4,§], V.R. Sonawane[5,**], Sharmila[6,††]

[1] *Karunya Institute of Technology and Sciences, Coimbatore, Tamil Nadu, India*
[2] *Department of Computer Science and Engineering, Shri Shankaracharya Institute of Professional Management & Technology, Raipur, India*
[3] *School of Engineering, Architecture and Interior Design, Amity University Dubai, P.O. Box 345019, Dubai International Academic City, United Arab Emirates*
[4] *Department of Computer Engineering, Sanjivani College of Engineering, Kopargaon, MH, India*
[5] *Department of Information Technology, Pune Vidyarthi Griha's College of Engineering & Shrikrushna S. Dhamankar Institute of Management, Nashik, India*
[6] *Department of ECE, Raj Kumar Goel Institute of Technology, Ghaziabad, India*

(Received 03 February 2026; revised manuscript received 18 April 2026; published online 29 April 2026)

Proton beam therapy is a promising modality for cancer treatment, offering high precision in dose delivery with minimal collateral damage. However, its therapeutic efficiency can be significantly enhanced through Nanoparticle (NPs) mediated sensitization, which strongly depends on the material properties of the NPs. This research investigates material-dependent variations in sensitization by combining computational and experimental approaches. A library of NPs, including noble metals (Au, Pt), transition metal oxides (TiO_2, Fe_3O_4), and hybrid composites (Au-TiO_2), was evaluated. Proton-NP interactions were modelled at the nanoscale using Monte Carlo-based Geant4-DNA simulations to predict secondary electron and radical yields, particularly for Au-TiO_2 hybrids. To mimic realistic tumor microenvironments, 3D tumor organoids were employed as biological models instead of conventional 2D cultures. Human-derived 3D tumor organoids were used to reproduce realistic tumor microenvironments. Proton irradiation generated Reactive Oxygen Species (ROS) formation, which was quantified by fluorescence assays, along with DNA double-strand break detection (γ-H_2AX and 53BP1). Proton irradiation (2-5 Gy) tests verified material-dependent ROS production, including Au-TiO_2 (18.2 μM, 180 %), Pt (15.6 μM, 156 %), and Au (12.8 μM, 128 %), standardized for surface area. Overall, the research presents a novel integrative framework for evaluating material-dependent variations in NP-mediated proton therapy sensitization.

Keywords: Proton beam therapy, Nanoparticle radio sensitization, Material-dependent variations, Monte Carlo (Geant4-DNA) simulation, 3D tumor organoids, Multi-omics profiling.

DOI: 10.21272/jnep.18(2).02023 PACS numbers: 87.55.Gh, 87.55.K –

1. INTRODUCTION

Radiotherapy is a popular cancer treatment that uses ionizing radiation to kill cancerous cells while preserving healthy tissues. It acts by causing direct or indirect Deoxyribonucleic Acid (DNA) damage, resulting in tumour control, decreased cancer growth, and increased patient life. Nanoparticles (NPs), especially High-Atomic-Number (High-Z) resources such as Gold (Au), improve radiotherapy by enhancing dose deposition by photoelectric effects, Auger particles, and residual radicals [1]. During radiotherapy, radiation reacts with biological macromolecules, producing free radicals that induce DNA breaks, deletions, and cross-linking. It also ionizes water in tissues, generating more radicals that damage macromolecules and cause cell death [2]. Gold NPs (GNPs) have High-Z and superior density absorption of energy compared to soft tissues, making them radio-sensitizing. This could improve tumour control, minimize adverse reactions, and enhance the longevity of patients in comparison to radiation treatment alone [3]. Mega Voltage (MV) electrons are better suited for tumour treatment than High-LET radiation. High-Z NPs improve photon radiotherapy by radio sensitization. X-rays excite inner electron shells, resulting in medium-to-high-energy Auger electrons, whereas High-LET atoms ionize outer layers, yielding lower-energy electrons. Under high stimulation, NPs produce more low-energy electrons than X-rays [4].

* Correspondence e-mail: williamacads@gmail.com
† apurv.verma1@gmail.com
‡ m.almakki1977@gmail.com
§ anilkumarbrahmane@gmail.com
** vijaysonawane11@gmail.com
†† apurv.verma1@gmail.com

Cite this article as: P. William et al., *J. Nano- Electron. Phys.* 18 No 2, 02023 (2026) https://doi.org/10.21272/jnep.18(2).02023

Radiation treatment includes External Beam Radiotherapy (EBRT), which uses high-energy proton or electron beams to treat local solid tumours, and Internal Radioisotope Therapy (RIT), which delivers therapeutic radioisotopes through intramuscular or intravenous carriers. RIT is capable of targeting both local and metastatic cancers. Almost half of those diagnosed with cancer undergo radiation treatments, either individually or in combination [5]. GNPs operate as radio sensitizers, increasing the local radiation dosage and producing secondary electrons and reactive species that damage DNA. Their high atomic number and biocompatibility enable them to maximize tumour cell killing while sparing healthy tissue [6]. Proton treatment effectively targets cancer cell DNA through the Bragg peak, minimizing harm to healthy tissues. The integration of boron-enhanced proton therapy, especially with boron-containing nanoparticles, enhances tumour targeting and boron delivery, potentially offering imaging and therapeutic advantages that can improve treatment efficacy and reduce adverse reactions [7]. Nanostructured radio sensitizers enhance radiation to improve local dosage while overcoming hypoxia and fast growth. Combining phototherapy with NP-based RT improves cancer care by significantly enhancing cancer fighting properties [8]. The research examines the material-dependent deviations in NPs-induced proton beam therapy sensitization using both computational simulation and experimental methods for assessing the way various NPs types, structures, and surface characteristics influence secondary electron development, destruction of DNA, and cellular responses in actual 3D tumour simulations.

The research is organized as follows: Section 1 offers the significant background of the research. Section 2 describes the related works, Section 3 presents the experimental design of the methodology, Section 4 presents the results and discussion, and Section 5 concludes the research.

2. RELATED WORK

Chinese Hamster Ovary-K1 (CHO-K1) cells were treated with 50 nm gold NPs and subjected to high-energy protons to evaluate radio sensitization [9]. The result demonstrated that the combination treatment increased cell death and chromosomal damage, validating the capability of Au NPs to improve the therapeutic efficiency of proton therapy. Gallic Acid-Gold NPs (GA-GNPs) were produced and administered to U251 glioblastoma cells, which were then exposed to radiation [10]. GA-GNPs dramatically enhanced radiation-driven cell death, caused cell cycle arrest at the Synthetic (S phase) and Gap 2/Mitosis (G2/M) phase, and triggered cell death, as demonstrated by elevated BCL-2-associated X protein (BAX) and reduced B-Cell Lymphoma 2 (BCL-2) levels, indicating a high sensitization capability. High-density Lipoprotein NPs (HDL NPs) were employed to deliver the radio-sensitizing microRNA, miR-34a, to head and neck cancer cells [11]. The improved radioactive effects reported in both 2D and 3D models substantiated HDL NPs' potential as an efficient delivery method for radio-sensitizing RNA. Radiotherapy (RT) was employed for widely Ionizing Radiation (IR) (X-rays) and intensive IR (protons) [12]. Cancer response is influenced by inheritance, gene expression, metabolism, environment, and non-malignant cells. Targeting these pathways aids in overcoming radio resistance and improving radiation efficacy Monte Carlo (MC) simulation, widely used for optimizing cancer dose [13], was performed with Geant4 on a 5 μm single-cell tumor model exposed to 100 MeV protons in a brain-like environment. Prostate Specific Membrane Antigen -targeted gold nanoparticles (PSMA-AuNPs) were utilized for radio sensitization of LNCaP prostate cancer cells that were exposed to 6 MV irradiation [14].

Depth-dependent effects were found, with Monte Carlo simulations and the local impact model correctly predicting cytoplasmic AuNP-induced dose augmentation and longevity of cells. Super-resolution Single Molecule Localization Microscopy (SMLM) and 3D confocal microscopy were used to examine the initial and final consequences of 10 nm-GNPs on DNA Double Strand Break (DSB) development [15]. PEG-coated boron nanoparticles (~ 25 nm) enhanced proton therapy by generating superoxide radicals [16]. It induces mitochondrial dehydration, triggering apoptosis, and upregulating 52 oxidative stress genes, thereby increasing tumor cell sensitivity to radiation and highlighting potential alpha particle effects. RPB7H NPs containing PROteolysis Targeting Chimera (PROTAC) prodrug BPA771 and HfO_2 were used to target Head and Neck Squamous Cell Carcinoma (HNSCC) tumors [17].

3. METHODOLOGY

The experimental design of methodology examines the NPs preparation, computational modelling, and biological model of 3D organoids, proton irradiation experiments, Monte Carlo simulations, and biological response assessments.

3.1 Nanoparticles (NPs) Preparation/Selection

A diverse set of NPs was chosen for examining the way material qualities affect proton treatment sensitivity. Noble metals, such as gold (Au) and platinum (Pt), were chosen because of their high atomic numbers and strong interaction with radiation. The surfactant-free Au, Pt, TiO_2, Fe_3O_4, and Au-TiO_2 NPs were synthesized using Laser Ablation in Liquid (LAL) and Laser Fragmentation (LFL) to achieve homogenous 3-5 nm particles. This green, ligand-free technique resulted in highly purified surfaces suitable for biomedical applications. Transmission Electron Microscopy (TEM) assessed particle size and shape, BET/ADC measured surface area, and XRD confirmed crystallinity. XPS/FTIR identified oxidation states and surface groups relevant to Reactive Oxygen Species (ROS) catalysis, while zeta potential ensured colloidal stability

Exemplary redox behaviors during ROS formation include the following Eqs 1 and 2.

$$Pt + H_2O \rightarrow .OH + H^+ + e^- \quad (1)$$

$$Au - TiO_2 + H_2 \rightarrow .OH + H_2O_2 \quad (2)$$

3.2 Computational Modeling

Monte Carlo-based Geant4-DNA simulations analysed proton-nanoparticle interactions on a nanoscale, focusing on secondary electron and free radical production. Noble metals like gold and platinum significantly emit electrons, leading to direct biomolecular ionization and water radiolysis, generating Reactive Oxygen Species (ROS) such as hydroxyl radicals. TiO_2 increases ROS generation via electron-hole pair formation, while Fe_3O_4 enhances radical production through Fenton-like reactions. Hybrid Au-TiO_2 nanoparticles exhibited a synergistic effect, enhancing oxidative stress through combined electron release and radical generation. The simulations provided insights into how material composition influences radio sensitization, suggesting hybrid nanoparticles as effective enhancers of proton therapy.

3.3 Biological Model-3D Tumor Organoids

Human-derived 3D malignant structures were used to create accurate tumor environments. DNA double-strand breaks were measured using γ-H_2AX and 53BP1 antibodies and high-resolution microscopy. ROS generation was measured using the fluorescent TA test, which allowed for correlation with computer predictions. Transcriptomic profiling using RNA-sequence identified genes involved in oxidative stress and cellular death, while proteomic testing using mass spectra connected protein-level reactions to ROS generation and destruction of DNA, establishing an extensive description of NPs-driven radio sensitization. The reaction of hydroxyl radicals (•OH) with Terephthalic Acid (TA) to form the fluorescent product 2-hydroxyterephthalic acid (2-OH-TA) is represented in Eq. 3.

$$TA + .OH -> 2 - OH - TA \quad (3)$$

3.4 Proton Irradiation Experiments

In proton irradiation tests, NP suspensions (Au, Pt, TiO_2, Fe_3O_4, Au-TiO_2) were subjected to therapeutic proton beams (2-5 Gy) to evaluate ROS formation. The TA fluorescent test (excitation 315 nm, emission 427 nm) was used to quantify hydroxyl radicals (•OH). $CaCl_2$ precipitation reduced quenching. ROS generation rose linearly with dosage. Table 1 provides NP-specific fluorescent dyes and properties. Fig. 2 shows the setup: proton beams irradiate 3D tumour organoids covered with NPs, and ROS production and DNA damage are evaluated in relation to NP type and proton dose.

Table 1 – Calibration parameters of fluorescent dyes used to quantify ROS production in proton irradiation experiments with different nanoparticle materials

Nanoparticle material	Dye used for ROS detection	Excitation λ [nm]	Emission λ [nm]	Concentration fluorescent product [nmol L^{-1}]
Gold (Au)	Terephthalic acid (TA)	315	429	10–500
Platinum (Pt)	Coumarin-3-carboxylic acid	326	445	10–500
Titanium dioxide (TiO_2)	Coumarin	326	456	10–500
Iron oxide (Fe_3O_4)	Amino and hydroxy phenyl fluorescein (APF, HPF)	470	510	10–500
Gold–Titanium dioxide hybrid (Au-TiO_2)	Terephthalic acid (TA)	315	429	10–500

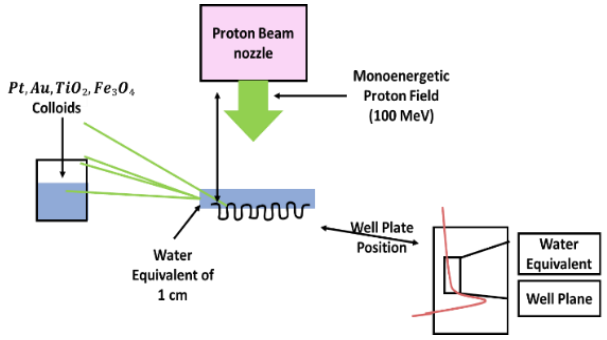

Fig. 2 – Experimental setups of the NPs mediated proton irradiation

3.5 Monte Carlo Simulations

Monte Carlo simulations employing the Geant4-DNA modeled nanoscale relationships among 3-5 nm spherical NPs and therapeutic proton beams (60-80 MeV). Substance parameters such as atomic quantity, mass, and ionization capability were used to estimate Secondary Electron yield (SE), electrical deposits, and water ionization. The outputs assessed ROS production and dose augmentation, offering theoretical direction for empirical nanoparticle identification and refinement for proton treatment.

3.6 Biological Response Assessment

Nanoparticle-mediated proton irradiation was analyzed using super-resolution microscopy for DNA damage and multi-omics profiling.

DNA damage visualization: Super-resolution microscopy was used to detect nanoscale DNA damage in tumor cells treated to proton irradiation with NPs. Double-strand breaks were identified and quantified using key markers like Phosphorylated Histone H2AX (γ-H2AX) and Tumor Protein p53-Binding Protein 1 (53BP1), providing an exact assessment of their amount and geographic distribution. This method offered extensive information about how different NPs increase proton-induced cytotoxicity by observing localized DNA damage at the subcellular level.

Multi-omics profiling: Transcriptomics (RNA-seq) and proteomics were employed to evaluate molecular responses to NP-mediated proton irradiation. RNA-seq identified alterations in genes involved in DNA repair,

apoptosis, oxidative stress, and cell cycle, while proteomics corroborated pathway activation. Integration revealed material-dependent heterogeneity in radio sensitization pathways responses.

4. RESULT

The results cover NP characterization, ROS generation under proton irradiation, and biological impacts. Particle size, surface area, and •OH yield was analysed, correlating ROS with DNA damage and apoptosis in 3D tumour organoids. Proton-NP interactions were simulated using Geant4-DNA in Python (16 GB RAM, 64-bit), while fluorescence assays and γ-H2AX/53BP1 detection measured ROS and DNA damage. Multi-omics profiling confirmed apoptosis pathways, integrating computational and experimental data to assess NP-mediated radio sensitization.

4.1 Particle Analysis

Laser Ablation in Liquid (LAL) generated noble metals (Au, Pt), metal oxides (TiO_2, Fe_3O_4), and hybrid Au-TiO_2 nanoparticles, which were then refined by Laser Fragmentation in Liquid (LFL) to yield monodisperse ~ 3-4 nm particles. To study surface effects, bigger Pt NPs (~ 22 nm) were extracted via centrifugation. TEM proved uniform size, whereas ADC assessed total surface area. NP suspensions were adjusted to approximately 9 cm^2/mL for direct comparison. Small and large Pt NPs (3-22 nm) produced similar •OH yields (~ 15 μM), while Au NPs (~ 3-20 nm) yielded ~ 13 μM, demonstrating that ROS generation depended on surface area rather than particle size or mass.

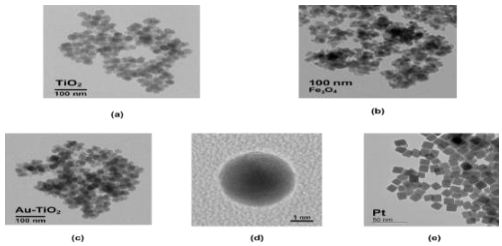

Fig. 3 – TEM images of (a) TiO_2, (b) Fe_3O_4, (c) Au-TiO_2 (d) Au NPs, and (e) Pt NPs

Fig. 3 shows several NPs of (a) TiO_2 NPs, generally spherical and somewhat consolidated, are depicted on a 100 nm scale. (b) Fe_3O_4 NPs look darker and more tightly packed at 100 nm. (c) Au-TiO_2 NPs have characteristics of both, with gold presumably incorporated or deposited on titanium. (d) A high-resolution image shows a single crystalline gold NPs around 5 nm in diameter, revealing its atomic structure. (e) Pt NPs have a characteristic cubic form, shown at a 50 nm scale, with well-defined facets.

Table 2 shows that the ROS yield for Pt (≈ 15 μM) and Au (≈ 13 μM) nanoparticles is virtually consistent when surface area is standardized, independent of particle size.

Table 2 – ROS yield vs Particle size

NP Type	Size (nm)	Mass Conc. (μg/mL)	Surface Area (cm^2/mL)	•OH Yield (μM)
Pt	3	10	9	15.8 ± 0.6
Pt	22	120	9	15.4 ± 0.5
Au	3	10	9	12.8 ± 0.5
Au	20	85	9	12.5 ± 0.4

4.2 NP-Dependent ROS Generation

ROS generation increased linearly with proton dose, suggesting a single-hit mechanism. At the same surface area, the •OH generation followed Eq. 4.

$$Au - TiO_2 > Pt > Au > Fe_3O_4 > TiO_2 \quad (4)$$

Hybrid nanoparticles produced approximately 1.8 times more •OH than the control, demonstrating surface catalytic function and beneficial effects outside the atomic count contributions. Table 3 shows material-dependent ROS generation at 5 Gy under equal surface area normalization. Hybrid Au-TiO_2 produced the highest yield (18.2 μM, 180%), followed by Pt (15.6 μM, 156%) and Au (12.8 μM, 128%), whereas Fe_3O_4 and TiO_2 showed comparatively lower enhancements.

Table 3 – NPs dependent ROS generation at 5 Gy

NP Type	Surface Area (cm^2/mL)	Mass Conc. (μg/mL)	•OH Yield (μM)	Relative Increase vs Control
Au-TiO_2	9	15	18.2 ± 0.8	180 %
Pt	9	14	15.6 ± 0.6	156 %
Au	9	12	12.8 ± 0.5	128 %
Fe_3O_4	9	13	10.4 ± 0.4	104 %
TiO_2	9	11	8.6 ± 0.3	86 %
Control	–	–	10 ± 0.2	100 %

4.3 DNA Damage and Apoptotic Correlation

Super-resolution imaging demonstrated 35-42 % more DNA Double-Strand Breaks (DSBs) in Pt and Au-TiO_2 medicated organoids compared to the control. Upregulation of oxidative stress genes (Nrf2 pathway). Higher levels of apoptotic proteins (Caspase-3 and Bax). The correlation between ROS increase and DNA damage demonstrates mechanistic agreement. Table 4 shows an apparent link between ROS production, DNA DSBs, and apoptotic signaling. Hybrid Au-TiO_2 NPs showed the highest reaction (42 % DSBs; Caspase-3: 2.8-fold), followed by Pt and Au. Elevated Bax and Caspase-3 levels confirm ROS-induced apoptosis, which is missing in the control group.

Table 4 – Correlation of ROS Yield with DNA Damage and Apoptotic Markers in NP-Treated Cells under Proton Irradiation

NP Type	•OH Yield (μM)	DNA DSBs (%)	Caspase-3 Fold Change	Bax Fold Change
Au–TiO_2	18.2 ± 0.8	42 ± 3	2.8	2.5
Pt	15.6 ± 0.6	38 ± 2	2.4	2.2
Au	12.8 ± 0.5	30 ± 2	1.8	1.7
Control	10 ± 0.2	0	1	1

Fig. 4 demonstrates the •OH yield was evaluated by particle size (a) and NP type under proton irradiation (b). Au-TiO_2 produced the most ROS, followed by Pt, Au, Fe_3O_4, TiO_2, and control. (c) Validates that •OH yield corresponds with DNA DSBs, with Au-TiO_2 showing the highest correlation, followed by Pt, Au, and control.

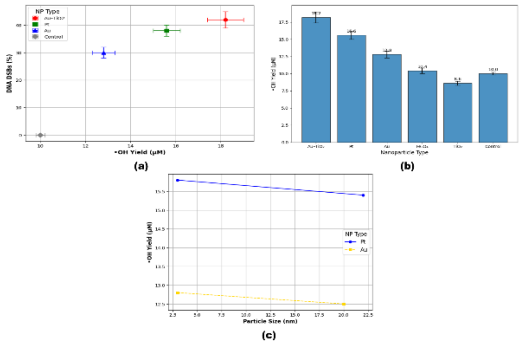

Fig. 4 – Representation of (a) OH yield vs particle size for different NPs at matched surface area, (b) •OH yield across NPs at 5 Gy and (c) OH yield vs DNA DSBs (%) for different NPs

5. DISCUSSION

Previous research has shown that nanoparticles can improve radio sensitivity across a variety of cancer models. Under proton irradiation, GNPs boosted cell death and chromosomal damage in CHO-K1 cells [9], whereas gallic acid-GNPs caused cell cycle arrest and apoptosis in U251 glioblastoma cells [10]. HDL NPs successfully transported radio-sensitizing miR-34a to head and neck cancer cells, increasing radiation efficacy in both 2D and 3D models [11]. Monte Carlo simulations also revealed dosage augmentation in relation to NPs concentration and distribution [12-13]. This research employed ligand-free Au, Pt, TiO_2, Fe_3O_4, and hybrid Au-TiO_2 NPs and measured their size, surface area, and stability. Proton irradiation of 3D tumor organoids revealed material-dependent ROS production, DNA double-strand breaks, and death. Hybrid Au-TiO_2 had the largest •OH output and apoptotic response.

6. CONCLUSION

The material-dependent variations in NPs-mediated proton therapy sensitization were clearly demonstrated in the research and assessed ROS generation, DNA damage, and molecular responses to identify optimal nanoparticle compositions for enhanced radio sensitization. NPs-mediated proton irradiation resulted in material-dependent ROS production and biological reactions. Hybrid Au-TiO_2 NPs had the highest •OH yield (18.2 μM, 180 %), followed by Pt and Au. Au-TiO_2 induced 42 % DSBs and increased Caspase-3 (2.8-fold) and Bax (2.5-fold), indicating apoptosis. The research focuses on in vitro 3D tumor organoids and nanoscale modeling, with no in vivo validation or long-term toxicity evaluation. Future research can look into in vivo models, optimizing NPs formulations for clinical use, and investigating combinatorial ways to improve proton therapy efficacy while avoiding off-target effects.

REFERENCES

1. W.B. Li, S. Stangl, A. Klapproth, M. Shevtsov, A. Hernandez, M.A. Kimm, J. Schuemann, R. Qiu, B. Michalke, M.A. Bernal, J. Li, *Cancers* **13** No 21, 5370 (2021) https://doi.org/10.3390/cancers13215370.
2. S. Yang, G. Han, Q. Chen, L. Yu, P. Wang, Q. Zhang, J. Dong, W. Zhang, J. Huang, *Int. J. Nanomed.* 239 (2021) https://doi.org/10.2147/IJN.S287523.
3. S.S. Mehrnia, B. Hashemi, S.J. Mowla, M. Nikkhah, A. Arbabi, *Radiation Oncology* **16** No 1, 33 (2021) https://doi.org/10.1186/s13014-021-01751-3.
4. I. Tremi, E. Spyratou, M. Souli, E.P. Efstathopoulos, M. Makropoulou, A.G. Georgakilas, L. Sihver, *Cancers* **13** No 13, 3185 (2021) https://doi.org/10.3390/cancers13133185.
5. W. Liu, B. Chen, H. Zheng, Y. Xing, G. Chen, P. Zhou, L. Qian, Y. Min, *Pharmaceutics* **13** No 11, 1757 (2021) https://doi.org/10.3390/pharmaceutics13111757.
6. H. Akhdar, R. Alanazi, N. Alanazi, A. Alodhayb, *Molecules* **27** No 16, 5290 (2022) https://doi.org/10.3390/molecules27165290.
7. I.N. Zavestovskaya, A.L. Popov, D.D. Kolmanovich, G.V. Tikhonowski, A.I. Pastukhov, M.S. Savinov, P.V. Shakhov, J.S. Babkova, A.A. Popov, I.V. Zelepukin, M.S. Grigoryeva, *Nanomaterials* **13** No 15, 2167 (2023) https://doi.org/10.3390/nano13152167.
8. M. Haque, M.S. Shakil, K.M. Mahmud, *Cancers* **15** No 6, 1892 (2023). https://doi.org/10.3390/cancers15061892.
9. C. Cunningham, M. de Kock, M. Engelbrecht, X. Miles, J. Slabbert, C. Vandevoorde, *Front. Public Health* **9**, 699822 (2021) https://doi.org/10.3389/fpubh.2021.699822.
10. Z. Jing, M. Li, H. Wang, Z. Yang, S. Zhou, J. Ma, E. Meng, H. Zhang, W. Liang, W. Hu, X. Wang, *IUBMB life* **73** No 2, 398 (2021) https://doi.org/10.1002/iub.2436.
11. P. Dehghankelishadi, M.F. Maritz, P. Badiee, B. Thierry, *Int. J. Pharmac.* **617**, 121585 (2022) https://doi.org/10.1016/j.ijpharm.2022.121585.
12. F. Busato, B.E. Khouzai, M. Mognato, *Int. J. Mol. Sci.* **23** No 18, 10211 (2022) https://doi.org/10.3390/ijms231810211
13. N. Alanazi, R. Alanazi, H. Akhdar, A. Alodhayb, *AIP Adv.* **12** No 10, (2022). https://doi.org/10.1063/5.0121239.
14. R.M. Schmidt, D. Hara, J.D. Vega, M.B. Abuhaija, W. Tao, N. Dogan, A. Pollack, J.C. Ford, J. Shi, *Pharmaceutics* **14** No 10, 2205 (2022) https://doi.org/10.3390/pharmaceutics14102205.
15. L. Dobešová, T. Gier, O. Kopečná, E. Pagáčová, T. Vičar, F. Bestvater, J. Toufar, A. Bačíková, P. Kopel, R. Fedr, G. Hildenbrand, *Pharmaceutics* **14** No 1, 166 (2022) https://doi.org/10.3390/pharmaceutics14010166.
16. A.L. Popov, D.D. Kolmanovich, N.N. Chukavin, I.V. Zelepukin, G.V. Tikhonowski, A.I. Pastukhov, A.A. Popov, A.E. Shemyakov, S.M. Klimentov, V.A. Ryabov, S.M. Deyev, *Molecules* **29** No 16, 3936 (2024) https://doi.org/10.3390/molecules29163936.
17. S. Zhang, Y. Lai, J. Pan, M. Saeed, S. Li, H. Zhou, X. Jiang, J. Gao, Y. Zhu, H. Yu, W. Zhang, *Adv. Mater.* **36** No 23, 2314132 (2024) https://doi.org/10.1002/adma.202314132.

Залежні від матеріалу варіації сенсибілізації протонного опромінення, опосередкованої наночастинками

P. William[1], A. Verma[2], M. Almakki[3], A.V. Brahmane[4], V.R. Sonawane[5], Sharmila[6]

[1] *Karunya Institute of Technology and Sciences, Coimbatore, Tamil Nadu, India*
[2] *Department of Computer Science and Engineering, Shri Shankaracharya Institute of Professional Management & Technology, Raipur, India*
[3] *School of Engineering, Architecture and Interior Design, Amity University Dubai, P.O. Box 345019, Dubai International Academic City, United Arab Emirates*
[4] *Department of Computer Engineering, Sanjivani College of Engineering, Kopargaon, MH, India*
[5] *Department of Information Technology, Pune Vidyarthi Griha's College of Engineering & Shrikrushna S. Dhamankar Institute of Management, Nashik, India*
[6] *Department of ECE, Raj Kumar Goel Institute of Technology, Ghaziabad, India*

Протонно-променева терапія є перспективним методом лікування раку, що пропонує високу точність доставки дози з мінімальним побічним збитком. Однак її терапевтичну ефективність можна значно підвищити за допомогою сенсибілізації, опосередкованої наночастинками (НЧ), яка сильно залежить від властивостей матеріалу НЧ. Це дослідження досліджує залежні від матеріалу варіації сенсибілізації шляхом поєднання обчислювальних та експериментальних підходів. Була оцінена бібліотека НЧ, включаючи благородні метали (Au, Pt), оксиди перехідних металів (TiO_2, Fe_3O_4) та гібридні композити (Au-TiO_2). Взаємодії протон-НЧ були змодельовані на нанорівні за допомогою моделювання Geant4-DNA на основі Монте-Карло для прогнозування виходу вторинних електронів та радикалів, особливо для гібридів Au-TiO_2. Для імітації реалістичних мікросередовищ пухлини як біологічні моделі використовувалися 3D-органоїди пухлини замість традиційних 2D-культур. Для відтворення реалістичних мікросередовищ пухлини використовувалися 3D-органоїди пухлини, отримані людиною. Протонне опромінення призвело до утворення активних форм кисню (АФК), що було кількісно визначено за допомогою флуоресцентних аналізів, а також виявлення дволанцюгових розривів ДНК (γ-H_2AX та 53BP1). Тести з протонним опроміненням (2-5 Гр) підтвердили залежне від матеріалу утворення АФК, включаючи Au-TiO_2 (18,2 мкМ, 180 %), Pt (15,6 мкМ, 156 %) та Au (12,8 мкМ, 128 %), стандартизовані за площею поверхні. Загалом, дослідження представляє нову інтегративну основу для оцінки залежних від матеріалу варіацій сенсибілізації до протонної терапії, опосередкованої наночастинками.

Ключові слова: Протонно-променева терапія, Радіосенсибілізація наночастинками, Матеріалозалежні варіації, Моделювання методом Монте-Карло (Geant4-DNA), 3D пухлинні органоїди, Мультиомічне профілювання.